

Coherent Axion Production through Laser Crystal Interaction

Zhan Bai,^{1,2,*} Xiangyan An,³ Yuqi Chen,⁴ Baifei Shen,⁵ Ruxin Li,⁶ and Liangliang Ji^{1,2,†}

¹State Key Laboratory of High Field Laser Physics,
Shanghai Institute of Optics and Fine Mechanics, Chinese Academy of Sciences

²CAS Center for Excellence in Ultra-intense Laser Science

³Tsung-Dao Lee Institute, Shanghai Jiao Tong University

⁴Institute of Theoretical Physics, Chinese Academy of Sciences

⁵Department of Physics, Shanghai Normal University

⁶Shanghai Tech University

(Dated: February 25, 2025)

We investigate the interaction between an optical laser and an ionic crystal and reveal coherent emission of axions through phase-match between laser and axion fields. Such emission is further enhanced by stacking thin crystal layers of half-wavelength thickness. Based on these findings, we propose a novel method for generating and detecting axions in terrestrial experiments, achieving up to a two-order-of-magnitude increase in transition probability compared to light-shining-through-wall (LSW) experiments with the same interaction region size. For an experimental length of 10 meters, this setup could lower the exclusion limit to $g_{a\gamma\gamma} \gtrsim 1.32 \times 10^{-11} \text{GeV}^{-1}$ with currently available laser technologies.

Introduction. Dark matter, a cornerstone of physics beyond the Standard Model, remains elusive (for review, see e.g. Ref. Bertone *et al.* [1]). Among its numerous candidates, axion is particularly promising. It was originally proposed to explain why the charge-parity violation term is extremely small in quantum chromodynamics (i.e. the strong CP problem) [2, 3], but was later found to be a perfect candidate for dark matter[4–6]. This dual relevance has spurred extensive experimental efforts, targeting both axions and axion-like particles.

Axion detection often relies on its coupling to electromagnetic fields. For instance, the CAST experiment detects solar axions by converting them into photons in a strong magnetic field[7, 8]. Similarly, CDMS experiments use germanium crystals, where axions are converted to photons through electric fields in atoms[9, 10], with Bragg condition-induced coherence enhancing signals[11].

Terrestrial experiments, such as light-shining-through-wall (LSW) setups, attempt to produce axions using the reverse of these mechanisms. Lasers interacting with magnetic fields produce axions, which then cross a wall and are reconverted to photons on the other side[12–14]. Other experiments, such as PVLAS[15, 16], use similar axion generation approaches. Enhancing axion production rates typically requires stronger or longer magnetic fields, but this approach is costly and technically challenging. Current LSW experiments use a magnetic field with $BL = 129 \text{Tm}$ [12] and plans to increase to $BL = 562 \text{Tm}$ [13].

To improve axion production, the strong electric fields inside crystals are harnessed, for instance, with X-rays interacting with crystals. Axions can be produced coherently when the Bragg condition is satisfied. However, absorption of X-ray photons by crystals limits the interaction distance to millimeter scale or even less [17–20],

far shorter than that in typical LSW setups ($\gtrsim 10 \text{m}$).

Inspired by these studies, we find a new approach to overcome these challenges and significantly boost the production rate of axions: optical laser interaction with transparent ionic crystals. Compared to X-rays, optical lasers possess higher photon densities and enable much longer propagation distance in crystals. Yet, in covalent crystals, Coulomb fields are shielded by electron clouds, making it highly localized within atoms. Such fields are difficult to be sensed by optical lasers with micrometer wavelength. We propose employing ionic crystals, wherein the Coulomb fields are much more widespread. Using this combination, we demonstrate that aligning light at specific angles and stacking thin crystal layers leads to a novel coherence mechanism, which is different from the Bragg-type enhancement. This approach significantly boosts axion production, offering a pathway to tighter constraints on axion coupling constants.

Coherent Axion Production in Medium. When a laser interacts with a point-like charge, the magnetic field of the laser is coupled with the Coulomb field, inducing overall non-zero $\mathbf{E} \cdot \mathbf{B}$, and axion field is excited according to wave equation [7] $(\partial_t^2 - \nabla^2 + m_a^2) a = g_{a\gamma\gamma} \mathbf{E} \cdot \mathbf{B}$, where a is the axion field, m_a is the axion mass, $g_{a\gamma\gamma}$ is the coupling constant, and \mathbf{E} and \mathbf{B} are the electric and magnetic field, respectively. Once the Coulomb fields are arranged in a periodic manner with scale length much smaller than the laser wavelength, the contribution from each are coherently superposed. In this case the axion production number is integrated[21]

$$N_a = \int \frac{d^3 \mathbf{k}_a}{(2\pi)^3} \frac{1}{2E_a} |\tilde{j}(\mathbf{k}_a^0, \mathbf{k}_a)|_{k_a^0=E_a}^2. \quad (1)$$

Here \mathbf{k}_a is the momentum of axion, $E_a = \sqrt{\mathbf{k}_a^2 + m_a^2}$ is the energy of axion, and $\tilde{j}(\mathbf{k}_a^0, \mathbf{k}_a)$ is the Fourier trans-

formation of the source term $j(t, \mathbf{r}) \equiv g_{a\gamma\gamma} \mathbf{E} \cdot \mathbf{B}$. We consider a linearly polarized laser whose magnetic field is $\mathbf{B} = \mathbf{B}_0 \cos(\omega t - \mathbf{k}_L \cdot \mathbf{r})$, with \mathbf{k}_L being the wave vector, and ω the circular frequency.

For many ions of charges q_s at locations \mathbf{r}_s , represented by the electric field $\mathbf{E} = \sum_s q_s (\mathbf{r} - \mathbf{r}_s) / (4\pi |\mathbf{r} - \mathbf{r}_s|^3)$, the conversion probability defined as $P = N_a/N_\gamma$ (N_γ is the laser photon number), is thus (for detailed derivation, see Appendix. A):

$$P_{\text{laser} \rightarrow a} = \frac{g_{a\gamma\gamma}^2}{S} \int d\Omega \frac{dP_{\text{single}}}{d\Omega} |\mathcal{T}|^2, \mathcal{T} \equiv \sum_s q_s e^{-i\Delta\mathbf{k} \cdot \mathbf{r}_s} \quad (2)$$

where S is the laser focal area, Ω is the solid angle, $dP_{\text{single}}/d\Omega$ is the differential conversion probability for a single charge at the origin, and $\Delta\mathbf{k} = \mathbf{k}_a - \mathbf{k}_L$ is the momentum transfer. It should be noted that while the \mathbf{E} field inside the ions can be different from point charge, the corresponding modification is negligible when the ion radius is much shorter than laser wavelength (see Appendix. C). The superposition of contributions from all ions are contained in the translation term \mathcal{T} .

Eq.(2) applies for charges at arbitrary positions. For a regularly placed crystal lattice, the translation term can be split into two parts: $\mathcal{T} \equiv \mathcal{T}_{\text{cell}} \cdot \mathcal{T}_{\text{lat}}$, defined as:

$$\mathcal{T}_{\text{cell}} \equiv \sum_c q_c e^{-i\Delta\mathbf{k} \cdot \delta\mathbf{r}_c}, \quad \mathcal{T}_{\text{lat}} \equiv \sum_l e^{-i\Delta\mathbf{k} \cdot \mathbf{r}_l} \quad (3)$$

where $\delta\mathbf{r}_c$'s are the relative positions of particle c in one cell, and \mathbf{r}_l 's are the reference coordinates for unit cells on lattice. From Eq.(3), it is clear that for optical lasers if the particles are all charge neutral atoms, $\mathcal{T}_{\text{cell}}$ vanishes and no axion signal is produced. Consider a simplest cell with two opposite charges $\pm q$ separating a distance $\delta\mathbf{r}$, the dipole moment leads to $\mathcal{T}_{\text{cell}} \approx iq\Delta\mathbf{k} \cdot \delta\mathbf{r}$, which is of order $\mathcal{O}(\omega|\delta\mathbf{r}|)$. Unlike in crystals of neutral atoms, such dipoles exist in ionic crystals where positive and negative charges are arranged in an interleaved pattern, leading to finite translation term for each cell $\mathcal{T}_{\text{cell}}$. Contributions from these cells at various locations are superposed following their phases in axion production, represented by the \mathcal{T}_{lat} term.

We consider an ionic crystal-calcium fluoride (CaF_2), as an illustration for coherent axion emission, although our discussion applies for all transparent ionic crystals. The CaF_2 crystal have face-centered-cubic(FCC) structure [22], where Ca^{2+} are located at the corners and the center of each face of the cube, and F^- occupy all the tetrahedral voids (holes) within the lattice. The interaction of laser pulse with the crystal structure is shown in Fig.1(a). In one cell, there are 4 Ca^{2+} and 8 F^- ions. The lattice constant is $d = 0.5451\text{nm}$, and the refractive index is $n = 1.43$ for laser wavelength $\lambda = 2\pi/\omega = 1064\text{nm}$ [23].

As shown in Fig.1(b), the laser injects into a crystal with an inclination angle α . From Eq.(3), we see that if

$\Delta\mathbf{k}$ is parallel to the transverse y -axis, cells with the same y -coordinates have the same phases, which contribute to a coherent enhancement. As the axion field travels along the longitudinal x -axis, \mathbf{k}_L , \mathbf{k}_a and $\Delta\mathbf{k}$ together form a phase-match condition, as shown in Fig. 1(b).

When axion mass $m_a \ll \omega$, the momentum of the outgoing axion satisfies $|\mathbf{k}_a| \approx \omega = |\mathbf{k}_L|/n$. The phase-match requires that $\alpha = \arccos \frac{1}{n}$, exactly the angle of full reflection. We can then complete the summation in \mathcal{T}_{lat} and its maximum value is:

$$|\mathcal{T}_{\text{lat}}^{\text{max}}|^2 = N_x^2 \frac{1 - \cos(N_y \omega d \tan \alpha)}{1 - \cos(\omega d \tan \alpha)} N_z^2, \quad (4)$$

where N_x , N_y and N_z is the number of unit cells along x , y and z direction, respectively. One notices coherent enhancement for large N_x and N_z , but periodically oscillates with N_y . It is because $\Delta\mathbf{k}$ is parallel to y -axis and as the phase $\Delta\mathbf{k} \cdot \mathbf{r}_l$ changes along the y direction, the signal undergoes coherent enhancement and coherent annihilation periodically.

Layer Structure. According to Eq.(4), the contribution from y direction reaches its maximum when $N_y^{\text{max}} \omega d \tan \alpha = (2M + 1)\pi$ for any integer M . However a larger M leads to a thicker crystal and larger focal area, which reduces conversion probability, as shown in Eq.(2). We will therefore take $M = 1$ for optimized axion conversion rate. For CaF_2 this means $N_y^{\text{max}} \approx 950$ and $L_y^{\text{max}} = N_y^{\text{max}} d \approx 518\text{nm}$, essentially a thin film. Further increase in N_y leads to the coherent annihilation and then enhancement and so on. The signals will oscillate according to Eq.(4).

It will be ideal if the annihilation phase $(2m - 1)\pi \leq N_y \omega d \tan \alpha \leq 2m\pi$ for any integer m , are inactivated to maintain continuous grow for large N_y . To do this, we propose stack multiple crystal layers along the y -axis, as is shown in Fig.1(c). Each layer is placed with a shift \mathbf{D} . They contribute to the translation term with a phase factor $\exp(-in\Delta\mathbf{k} \cdot \mathbf{D})$ for the n -th layer. For best coherence, we require that $\Delta\mathbf{k} \cdot \mathbf{D} = 2N\pi$, where N is an arbitrary integer. Similar to the choice of M , we take $N = 1$ for smallest focal area and largest conversion probability. We then have $D_y = (2\pi/\omega) \cot \alpha$. We also want each layer on the same phase front of the laser, i.e. $\mathbf{D} \perp \mathbf{k}_L$, so we have $D_x = D_y / \cot \alpha = 2\pi/\omega$.

The spaces between displaced thin ionic crystal layers should be filled with other transparent materials for stability of the structure. Those materials should be atom crystals that are inactive for axion production to avoid coherent annihilation (see Appendix. C). In order for the light to propagate between layers, the supporting layers should have similar refractive index. For example, the SiO_2 crystal has $n = 1.45$ [23], which is close to CaF_2 .

In this stacked layers, since our choice of propagating direction $\alpha = \arccos 1/n$ is the critical angle for total reflection, the laser keeps reflecting while propagating along

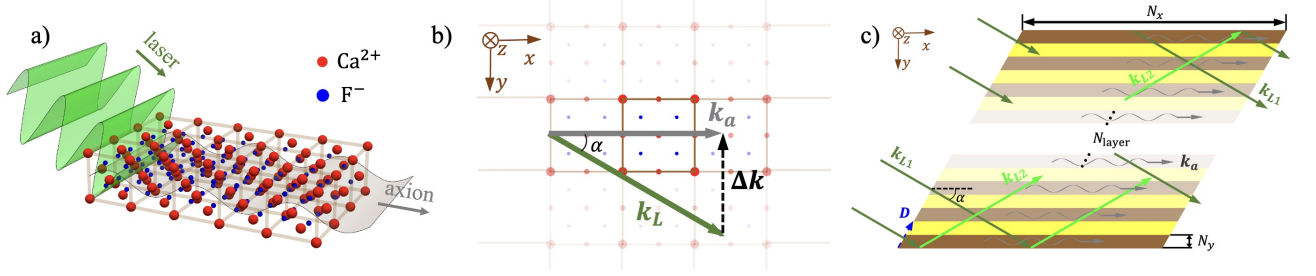


Figure 1. *Panel (a)*: A schematic figure for the coherent production of axion in laser-crystal interactions. The green and gray surfaces indicate the incoming laser and the outgoing axion fields, respectively. The red and blue spheres indicate positive and negative ions, respectively. Each brown cubic represents a unit cell. *Panel (b)*: A side view of panel (a). The brown squares indicate the crystal cells. \mathbf{k}_L and \mathbf{k}_a are the wave vectors for incoming light and outgoing axion, respectively. *Panel (c)*: A schematic figure for the stacking of thin crystal films. The brown layers represent the ionic crystal materials. Every brown layer has $N_x \times N_y \times N_z$ lattice cells, and each layer shifts a constant \mathbf{D} in the direction perpendicular to the laser direction $\mathbf{k}_{L1} = \mathbf{k}_L$. In the uppermost and lowermost layers, we present a schematic figure for the reflection. Mention that \mathbf{k}_{L1} is the wave vector for the incident laser and also the laser reflected by the upper boundary, and \mathbf{k}_{L2} is the wave reflected by the lower boundary. The yellow areas are the supporting material.

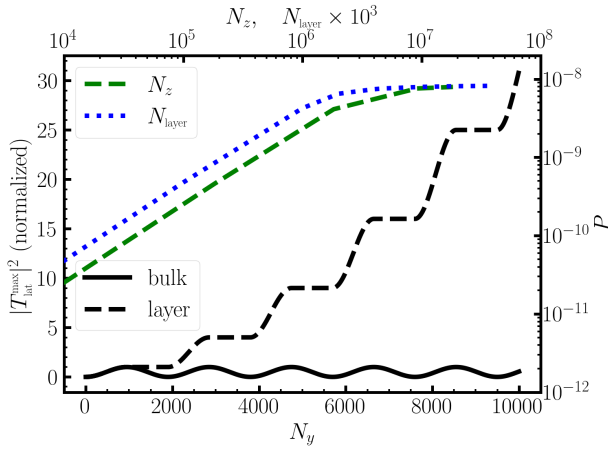


Figure 2. Scaling behavior with the increase of crystal sizes. Black lines (left and bottom axes) show $|\mathcal{T}_{\text{lat}}|^2$ versus N_y . The solid line represents oscillations in a complete bulk crystal (Eq.(4)), while the dashed line shows growth when layer structure is used. The left y -axis is normalized so that the maximum value for the black solid line is 1. Colored lines (top and right axes) indicate conversion probability growth with increasing N_z and N_{layer} .

x direction, on the uppermost and lowermost layer surface, as indicated in Fig.1(c). This is equivalent to a rectangular waveguide working in transverse electronic (TE) mode. We can then treat the wave function as two propagating plane waves, with wave vectors $\mathbf{k}_{L1} = n\omega(\cos \alpha, \sin \alpha, 0)$ and $\mathbf{k}_{L2} = n\omega(\cos \alpha, -\sin \alpha, 0)$. Substituting into Eq.(1), we can derive the conversion probability.

The detailed derivation and explicit formula for the conversion probability can be found in Appendix. A3 and Eq.(A28). Here we only analyze the scaling behavior qualitatively. Eq.(4) presents the maximum value of $|\mathcal{T}_{\text{lat}}|^2$ when the phase-match condition is satisfied. It oscillates periodically if N_y increases monotonically, as shown in Fig. 2 with the black solid line. However, if we keep only the increasing region and inactivate the de-

creasing region, i.e., if we use layer structure, the $|\mathcal{T}_{\text{lat}}|^2$ will increase continuously. The summation of all layers will contribute a factor $[\sum_n \exp(-in\Delta\mathbf{k} \cdot \mathbf{D})]^2 \approx N_{\text{layer}}^2$ to $|\mathcal{T}_{\text{lat}}^{\text{max}}|^2$, where N_{layer} is the total number of layers, as shown in Fig. 2 with the black dashed line.

$|\mathcal{T}_{\text{lat}}|^2$ is strongly peaked near phase-match condition, which leads to extremely collimated axion emission with divergence angle $\Delta\Omega$. The integration in Eq.(2) is then approximately $P \propto \frac{1}{S} N_{\text{layer}}^2 |\mathcal{T}_{\text{cell}} \mathcal{T}_{\text{lat}}^{\text{max}}|^2 \Delta\Omega$. The divergence angle, $\Delta\Omega$, is proportional to λ^2/S . Since $S \propto N_{\text{layer}} N_z$, we can see the N_{layer}^2 dependence and N_z^2 dependence in $|\mathcal{T}_{\text{lat}}^{\text{max}}|^2$ are canceled by the focal area S^2 . Therefore, the conversion probability only scales as N_x^2 , and does not rely on N_z and N_{layer} , as long as the crystal is large enough and enter the scaling region.

We numerically calculate the conversion probability for $g_{a\gamma\gamma} = 10^{-7} \text{GeV}^{-1}$ and $m_a = 10^{-6} \text{eV}$, with different crystal sizes, as shown in Fig. 2 with colored lines. $N_x = 1.83 \times 10^{10}$ and $N_y = 950$ is fixed for these two lines, and the conversion probability clearly increases when N_z and N_{layer} are small, but saturates for $N_z \gtrsim 10^7$ and $N_{\text{layer}} \gtrsim 3 \times 10^3$.

Therefore, we consider $N_x = 1.83 \times 10^9$, $N_y = 950$, $N_z = 9.17 \times 10^6$, and $N_{\text{layer}} = 4.8 \times 10^3$, so that the target is a thin rod with size $1\text{m} \times 5\text{mm} \times 5\text{mm}$. The conversion probability is $P_{\text{laser} \rightarrow a}^{\text{1m}} = 8.53 \times 10^{-11}$. If we increase N_x to 1.83×10^{10} , i.e. consider a 10-meter-long rod, the conversion probability will be $P_{\text{laser} \rightarrow a}^{\text{10m}} = 7.58 \times 10^{-9}$. For comparison, in LSW experiment[12], the conversion probability is $P_{\text{OSQAR}} = 4.06 \times 10^{-11}$ for the same axion mass and coupling, with magnetic field of length $L = 14.3\text{m}$. Therefore, if the length scale of the crystal is of the same order as the magnetic field length for LSW experiment, the conversion probability can be two order of magnitude higher.

Reconversion. As we have stated, the axion beam is highly collimated. For the crystal size we use, the divergence is around $\Delta\theta \lesssim 3 \times 10^{-5} \pi$. This highly directional

axion beam is favorable for reconversion into light for detection. By injecting the axion into another crystal, they will convert back to light by interacting with the Coulomb field of the ions. For crystals inside a rectangular waveguide, TE mode will be excited. The physical picture is the inverse of axion production, and phase match condition is identical, so the layer structure is required. The detailed derivation is shown in Appendix.B and Eq.(B16).

We again consider $g_{a\gamma\gamma} = 10^{-7}\text{GeV}^{-1}$ and $m_a = 10^{-6}\text{eV}$ for comparison. For a CaF_2 stick with size $1\text{m} \times 5\text{mm} \times 5\text{mm}$, i.e. with $N_x = 1.83 \times 10^9$, $N_y = 950$, $N_z = 9.17 \times 10^6$, and $N_{\text{layer}} = 4.8 \times 10^3$, the conversion probability is $P_{a \rightarrow \gamma}^{1\text{m}} = 1.85 \times 10^{-10}$. If we further increase the length to 10m, we have $P_{a \rightarrow \gamma}^{10\text{m}} = 1.85 \times 10^{-8}$.

Experimental Design and Exclusion Line. The schematic figure for the experimental setups are shown in the upper panel of Fig. 3. On the left is interaction region, where light converts to axions. The light is reflected between two mirrors to enhance photon number. On the right is detecting crystal, where the axions convert back to light and then be detected. An opaque wall blocks the light while axions can cross it freely, as in LSW experiments. We consider the same laser as reported in ALPS-II[24], with effective laser power at $P_{\text{laser}} = 150\text{ kW}$, wavelength $\lambda = 1064\text{ nm}$ in vacuum, corresponding to photon energy $\omega = 1.17\text{ eV}$. For 1 year experiment with running time $3 \times 10^7\text{ s}$, the total photon number is $N_{\gamma}^{\text{laser}} = 2.41 \times 10^{31}$. The event number is:

$$N_{\text{event}} = N_{\gamma}^{\text{laser}} P_{\text{laser} \rightarrow a} P_{a \rightarrow \gamma} \left(\frac{g_{a\gamma\gamma}}{10^{-7}\text{GeV}^{-1}} \right)^4.$$

Using $N_{\text{event}} = 1$ as criterion, we have $g_{a\gamma\gamma} \geq 1.29 \times 10^{-10}\text{GeV}^{-1}$ for $L = 1\text{m}$ and $g_{a\gamma\gamma} \geq 1.32 \times 10^{-11}\text{GeV}^{-1}$ for $L = 10\text{m}$, in the limit of $m_a \ll \omega$. The complete exclusion line should be obtained by scanning the $g_{a\gamma\gamma} - m_a$ plane, and is shown in the lower panel of Fig. 3.

Conclusion. In this letter, we present a novel way to create axions and ALPs in terrestrial experiment. We use optical laser to interact ionic crystal, and find a coherent enhancement at the phase-matching condition. These coherence is similar to those in previous studies[17–20, 26], and further increase of the coherence is achieved by the use of thin film layers. Under our design, the conversion probability can be 2 orders of magnitude larger than traditional LSW experiment, as long as the size of the crystal is the same as the magnetic fields in LSW experiment. We estimate that our proposal is able to push the axion exclusion line down to $g_{a\gamma\gamma} \gtrsim 1.32 \times 10^{-11}\text{GeV}^{-1}$.

Current coating technique has already enabled the stacking of 1000 layers, with the thickness of single or multilayers from 5 nm to $10\text{ }\mu\text{m}$, and the size of the film of tens of square centi-meters[27]. Our design is therefore possible with current or near-future technique.

Acknowledgments. This work is supported by National Natural Science Foundation of China (No.

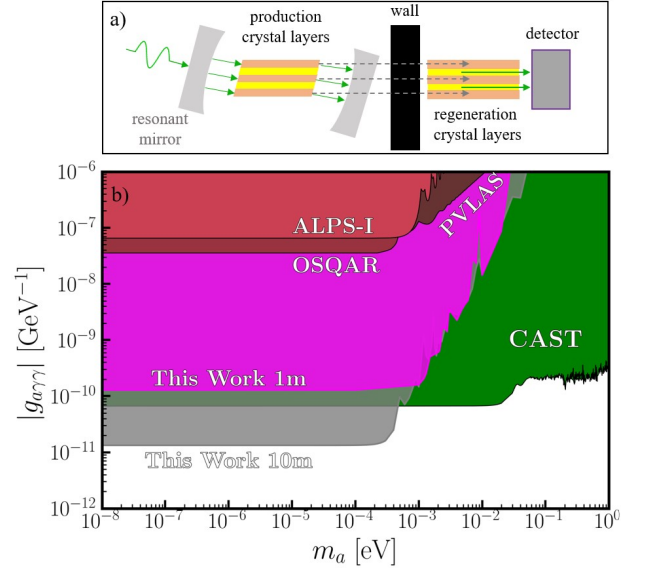


Figure 3. *Upper panel:* Schematic figures for the experimental setup. *Lower panel:* The exclusion line for our proposal. The shaded pink region is excluded using 1m conversion and reconversion length, and the shaded gray region is excluded using 10m conversion and reconversion region. The exclusion lines from LSW[12, 14], PVLAS[15] and CAST[8] experiments are also given as comparison. The figure is plotted using Axion Limits[25].

12388102), the Strategic Priority Research Program of the Chinese Academy of Sciences (No. XDB0890303), the CAS Project for Young Scientists in Basic Research (No. YSBR060). We thank Yin Hang and Lianghong Yu from SIOM, CAS, and Zheng Gong from ITP, CAS for helpful discussion.

* baizhan@siom.ac.cn

† jill@siom.ac.cn

- [1] G. Bertone, D. Hooper, and J. Silk, *Phys. Rept.* **405**, 279 (2005), [arXiv:hep-ph/0404175](#).
- [2] R. D. Peccei and H. R. Quinn, *Phys. Rev. Lett.* **38**, 1440 (1977).
- [3] R. D. Peccei and H. R. Quinn, *Phys. Rev. D* **16**, 1791 (1977).
- [4] M. Dine and W. Fischler, *Phys. Lett. B* **120**, 137 (1983).
- [5] L. F. Abbott and P. Sikivie, *Phys. Lett. B* **120**, 133 (1983).
- [6] J. Preskill, M. B. Wise, and F. Wilczek, *Phys. Lett. B* **120**, 127 (1983).
- [7] S. Andriamonje *et al.* (CAST), *J. Cosmol. Astropart. Phys.* **04**, 010, [arXiv:hep-ex/0702006](#).
- [8] V. Anastassopoulos, others, and CAST Collaboration (CAST collaboration), *Nat. Phys.* **13**, 584 (2017).
- [9] Z. Ahmed *et al.*, *Phys. Rev. Lett.* **103**, 141802 (2009).
- [10] M. F. Albakry *et al.* (SuperCDMS), *A Strategy for Low-Mass Dark Matter Searches with Cryogenic Detectors in the SuperCDMS SNOLAB Facility* (2023), [arXiv:2203.08463](#).
- [11] R. J. Creswick, F. T. Avignone, III, H. A. Farach, J. I. Collar, A. O. Gattone, S. Nussinov, and K. Zioutas, *Phys.*

- Lett. B **427**, 235 (1998), [arXiv:hep-ph/9708210](#).
- [12] R. Ballou *et al.* (OSQAR Collaboration), *Phys. Rev. D* **92**, 092002 (2015).
 - [13] T. Kozlowski *et al.*, Design and Performance of the ALPS II Regeneration Cavity (2024), [arXiv:2408.13218](#).
 - [14] K. Ehret *et al.*, *Phys. Lett. B* **689**, 149 (2010).
 - [15] F. Della Valle *et al.*, *Eur. Phys. J. C* **76**, 24 (2016).
 - [16] A. Ejlli *et al.*, *Phys. Rep.* **871**, 1 (2020).
 - [17] W. Buchmuller and F. Hoogeveen, *Phys. Lett. B* **237**, 278 (1990).
 - [18] B. L. Henke, E. M. Gullikson, and J. C. Davis, *Atom. Data Nucl. Data Tabl.* **54**, 181 (1993).
 - [19] T. Yamaji, T. Yamazaki, K. Tamasaku, and T. Namba, *Phys. Rev. D* **96**, 115001 (2017), [arXiv:1709.03299](#).
 - [20] J. W. D. Halliday *et al.*, *Phys. Lett. Lett.* **134**, 055001 (2025), [arXiv:2404.17333](#).
 - [21] M. E. Peskin, *An Introduction to Quantum Field Theory* (Westview Press, 1995).
 - [22] Calcium fluoride, https://en.wikipedia.org/w/index.php?title=Calcium_fluoride&oldid=1256066213 (2024).
 - [23] M. N. Polyanskiy, *Sci. Data* **11**, 94 (2024).
 - [24] ALPS II, https://alps.desy.de/our_activities/axion_wisp_experiments/alps_ii/.
 - [25] C. O'Hare, *Cajohare/AxionLimits: AxionLimits* (2020).
 - [26] S. Matsumoto, J. Sheng, and C.-Y. Xing, *Detection of Dark Matter Coherent Scattering via Torsion Balance with Test Bodies of Different Sizes* (2024), [arXiv:2409.09950 \[hep-ph\]](#).
 - [27] Helios Sputtering Tool | Bühler Leybold Optics | Bühler Group, https://www.buhlergroup.cn/global/en/products/leybold_optics_heliosseriesprecisionopticsvacuumcoater.html.
 - [28] N. Baddour, in *Advances in Imaging and Electron Physics*, Advances in Imaging and Electron Physics, Vol. 165, edited by P. W. Hawkes (Elsevier, 2011) pp. 1–45.
 - [29] X. An, M. Chen, J. Liu, Z. Sheng, and J. Zhang, *Matter Radiat. Extremes* **9**, 067204 (2024), [arXiv:2406.16796](#).
 - [30] J. D. Jackson, *Classical Electrodynamics*, 3rd ed. (JOHN WILEY & SONS, INC., 1999).

Appendix A: Axion Production in Coulomb Potentials

In this appendix, we will consider the interaction between the laser and the ions, where the ions are components of some ionic crystal. We mention that there is a variety of ionic crystals widely used in laser science. For example, the calcium fluoride (CaF_2) crystal is transparent and can be used as light amplifier. When a laser is injected into such crystals, its magnetic component will interact with the Coulomb field of the ions, contributing a non-zero axion source $\mathbf{E} \cdot \mathbf{B}$.

The Lagrangian for ALP is:

$$\mathcal{L} = \frac{1}{2} \partial_\mu a \partial^\mu a - \frac{1}{2} m_a^2 a^2 - \frac{1}{4} F_{\mu\nu} F^{\mu\nu} - \frac{1}{4} g_{a\gamma\gamma} a F_{\mu\nu} \tilde{F}^{\mu\nu}, \quad (\text{A1})$$

where a is the axion field with mass m_a , $F_{\mu\nu} \equiv \partial_\mu A_\nu - \partial_\nu A_\mu$ is the field strength of the electromagnetic field A_μ , $\tilde{F}_{\mu\nu} \equiv 1/2 \varepsilon_{\mu\nu\rho\sigma} F_{\rho\sigma}$ is its dual, and $g_{a\gamma\gamma}$ is the coupling constant with the dimension of inverse energy. We mention that $-1/4 F_{\mu\nu} \tilde{F}^{\mu\nu} = \mathbf{E} \cdot \mathbf{B}$ where \mathbf{E} is the electric field and \mathbf{B} is the magnetic field. The field equation for $a(t, \mathbf{r})$ is derived by differentiating the Lagrangian:

$$(\partial_t^2 - \nabla^2 + m_a^2) a = g_{a\gamma\gamma} \mathbf{E} \cdot \mathbf{B}. \quad (\text{A2})$$

Eq.(A2) is an ordinary Klein-Gordon equation, and the axion field $a(t, \mathbf{r})$ can be solved when the external source $\mathbf{E} \cdot \mathbf{B}$ is known. The axion number produced in classical source is (see, e.g., Sec.2.4 of [21]):

$$N_a = \int \frac{d^3 \mathbf{k}_a}{(2\pi)^3} \frac{1}{2E_a} |\tilde{j}(k_a^0, \mathbf{k}_a)|_{k_a^0=E_a}^2, \quad (\text{A3})$$

where $E_a = \sqrt{\mathbf{k}_a^2 + m_a^2}$ and $\tilde{j}(k_a)$ is the Fourier transformation of the external source:

$$\tilde{j}(k_a^0, \mathbf{k}_a) = \int dt d^3 \mathbf{r} e^{ik_a^0 t} e^{-i\mathbf{k}_a \cdot \mathbf{r}} j(t, \mathbf{r}),$$

where $j(t, \mathbf{r}) = g_{a\gamma\gamma} \mathbf{E} \cdot \mathbf{B}$.

1. conversion probability in Medium

We consider a linearly polarized laser propagating along the x -axis. The magnetic component is then:

$$\mathbf{B} = (0, B_0 \cos(\omega t - k_L x), 0). \quad (\text{A4})$$

where ω is the frequency of the laser, and \mathbf{k}_L is the corresponding wave vector, $k_L \equiv |\mathbf{k}_L|$. In crystals, we have refractive index $n = k_L/\omega > 1$, i.e. $k_L > \omega$.

Assuming that this laser passes through a set of point particles with charges $\{q_s\}$ located at $\{\mathbf{r}_s\}$. The corresponding electric field is:

$$\mathbf{E} = \sum_s \mathbf{E}_s = \sum_s \frac{q_s}{4\pi |\mathbf{r} - \mathbf{r}_s|^3} (\mathbf{r} - \mathbf{r}_s). \quad (\text{A5})$$

We mention that $\mathbf{r} = (x, y, z)$. The classical source for axion production is then $j(t, \mathbf{r}) = \sum_s g_{a\gamma\gamma} \mathbf{E}_s \cdot \mathbf{B}$, and its Fourier transformation is:

$$\tilde{j}(k_a^0, \mathbf{k}_a) \equiv \frac{g_{a\gamma\gamma} B_0}{4} \delta(k_a^0 - \omega) \tilde{j}(\mathbf{k}_a) \mathcal{T}(\mathbf{k}_a; \{\mathbf{r}_s\}) \quad (\text{A6})$$

where we have defined:

$$\tilde{j}(\mathbf{k}_a) = \int d^3\mathbf{r} \exp[-i\mathbf{k}_a \cdot \mathbf{r}] j(\mathbf{r}), \quad j(\mathbf{r}) = \frac{e^{ik_L x}}{|\mathbf{r}|^3} y. \quad (\text{A7})$$

and

$$\mathcal{T}(\mathbf{k}_a; \{\mathbf{r}_s\}) \equiv \sum_s q_s e^{-i\mathbf{k}_a \cdot \mathbf{r}_s} e^{ik_L x_s}. \quad (\text{A8})$$

The expression for $\tilde{j}(\mathbf{k}_a^0, \mathbf{k}_a)$ means that, we can separate the source term into two parts. One is $\tilde{j}(\mathbf{k}_a)$, which contains the information for one single point charge. Another part, $\mathcal{T}(\mathbf{k}_a; \{\mathbf{r}_s\})$, is a summation of phases, which contains the information for charge positions. We will in the following refer to \mathcal{T} as “translation term”.

The expression for $\tilde{j}(\mathbf{k}_a)$ can be derived by performing a Fourier transformation in cylindrical coordinate (see [28]), where $k_{ar} = k_a \sin \theta$, $k_{ay} = k_{ar} \cos \phi$ and $k_{az} = k_{ar} \sin \phi$. We have:

$$\tilde{j}(\mathbf{k}_a) = -4\pi i \frac{k_{ay}}{k_{ar}^2 + (k_{ax} - k_L)^2}. \quad (\text{A9})$$

Substituting into the expression for $\tilde{j}(\mathbf{k}_a^0, \mathbf{k}_a)$, and writing in vector form, we have:

$$\tilde{j}(\mathbf{k}_a^0, \mathbf{k}_a) = -\pi i g_{a\gamma\gamma} B_0 \delta(k_a^0 - \omega) \frac{\Delta k_y}{(\Delta \mathbf{k}^2)^2} \left[\sum_s q_s e^{-i(\mathbf{k}_a - \mathbf{k}_L) \cdot \mathbf{r}_s} \right] \quad (\text{A10})$$

where $\Delta \mathbf{k} = \mathbf{k}_a - \mathbf{k}_L$. Then, using Eq.(A3), we can calculate the axion number. Mention that a special care should be taken for the delta function. We have:

$$\delta(\omega)^2 = \frac{T}{2\pi} \delta(\omega), \quad (\text{A11})$$

where T is the large time period during which interaction is present. We can then integrate over the remaining delta function using $d^3\mathbf{k}_a = |\mathbf{k}_a|^2 d|\mathbf{k}_a| \sin \theta d\theta d\phi$, and have:

$$N_a = \frac{g_{a\gamma\gamma}^2 B_0^2}{32\pi^2} T |\mathbf{k}_a|^3 \int_0^\pi d\theta \int_0^{2\pi} d\phi \frac{\cos^2 \phi \sin^3 \theta}{(\Delta \mathbf{k}^2)^2} \left| \sum_s q_s e^{-i\Delta \mathbf{k} \cdot \mathbf{r}_s} \right|^2, \quad (\text{A12})$$

where $|\mathbf{k}_a| = \sqrt{\omega^2 - m_a^2}$.

For photon of energy ω , the number of incoming photon during time T is:

$$N_\gamma = \rho_\gamma S v_\gamma T = \frac{B_0^2}{\omega} S \frac{1}{n} T, \quad (\text{A13})$$

where S is the laser focal area. The conversion probability is:

$$P_{\text{laser} \rightarrow a} \equiv \frac{N_a}{N_\gamma} = \frac{g_{a\gamma\gamma}^2 k_L}{32\pi^2 S} |\mathbf{k}_a|^3 \int_0^\pi d\theta \int_0^{2\pi} d\phi \frac{\cos^2 \phi \sin^3 \theta}{(\Delta \mathbf{k}^2)^2} |\mathcal{T}(\Delta \mathbf{k}; \{\mathbf{r}_s\})|^2. \quad (\text{A14})$$

2. Incident Angle for Coherent Enhancement

From Eq.(A14), we can see that the conversion probability is related to $|\mathcal{T}|^2$, where \mathcal{T} is the translation term as defined in Eq.(A8). This term contains a summation over all charges, so it is possible to grow when the crystal volume

increases, as long as the phase of each charge accumulates rather than cancels out. In crystals, the unit cells and the charges distribute regularly, so we can rewrite the translation term as:

$$\begin{aligned}\mathcal{T} &= \sum_s q_s e^{-i(\mathbf{k}_a - \mathbf{k}_L) \cdot \mathbf{r}_s} \\ &= \left[\sum_c q_c e^{-i(\mathbf{k}_a - \mathbf{k}_L) \cdot \delta \mathbf{r}_c} \right] \left[\sum_l e^{-i(\mathbf{k}_a - \mathbf{k}_L) \cdot \mathbf{r}_l} \right] \\ &\equiv \mathcal{T}_{\text{cell}} \cdot \mathcal{T}_{\text{lattice}}\end{aligned}$$

where \mathbf{r}_l 's are the coordinates for unit cells, and $\delta \mathbf{r}_c$'s are the relative position of particle c in one cell. The summation of c runs over all particles in one unit cell, and summation of l runs over all coordinates of unit cells. We then divide the translation term into the contribution from cell and from lattice. As we can see, the contribution from cell, $\mathcal{T}_{\text{cell}}$, is a constant term and do not accumulate with the increase of crystal size. Therefore, we are more interested in the $\mathcal{T}_{\text{lattice}}$ term.

In order to coherently enhance the axion production, we want to find a specific direction, where multiple lattice sites have the same phase $i(\mathbf{k}_a - \mathbf{k}_L) \cdot \mathbf{r}_l$. To do this, we rotate the crystal, so that the incoming laser is not perpendicular to the crystal surface, as shown in Fig. 1.

We consider crystal whose unit cell is cubic. In “crystal coordinate” where the cells align along axes, the positions of the unit cells are:

$$\mathbf{r}' = (i_1, i_2, i_3) d, \quad i_1, i_2, i_3 \in \mathbb{Z}, \quad (\text{A15})$$

where d is the lattice constant. We use prime notation to denote coordinate in “crystal coordinate”. In “laser coordinate” where the laser is propagating along x -direction, the positions are:

$$\mathbf{r} = (i_1 \cos \alpha + i_2 \sin \alpha, -i_1 \sin \alpha + i_2 \cos \alpha, i_3) d, \quad (\text{A16})$$

where α is the inclination angle. We use $\Delta \mathbf{k} = \mathbf{k}_a - \mathbf{k}_L$ for short notation, and the translation term can be written as:

$$\begin{aligned}\mathcal{T}_{\text{lattice}} &= \sum_l \exp[-i(\Delta k_x x_l + \Delta k_y y_l + \Delta k_z z_l)] \\ &= \sum_{i_1=0}^{N_x-1} \sum_{i_2=0}^{N_y-1} \sum_{i_3=0}^{N_z-1} \exp[-i\Delta k_x d(i_1 \cos \alpha + i_2 \sin \alpha) - i\Delta k_y d(-i_1 \sin \alpha + i_2 \cos \alpha) - i\Delta k_z i_3 d] \\ &= \sum_{i_1=0}^{N_x-1} \exp[-i(\Delta k_x \cos \alpha - \Delta k_y \sin \alpha) i_1 d] \sum_{i_2=0}^{N_y-1} \exp[-i(\Delta k_x \sin \alpha + \Delta k_y \cos \alpha) i_2 d] \sum_{i_3=0}^{N_z-1} \exp[-i\Delta k_z i_3 d]\end{aligned}$$

where N_x , N_y and N_z is the number of unit cells along x' , y' and z' direction, respectively. The summation over all lattice sites can be expressed as three geometric series summations, which can be easily done and we have:

$$\begin{aligned}\mathcal{T}_{\text{lattice}} &= \left(\frac{1 - \exp[-i(\Delta k_x \cos \alpha - \Delta k_y \sin \alpha) N_x d]}{1 - \exp[-i(\Delta k_x \cos \alpha - \Delta k_y \sin \alpha) d]} \right) \\ &\quad \times \left(\frac{1 - \exp[-i(\Delta k_x \sin \alpha + \Delta k_y \cos \alpha) N_y d]}{1 - \exp[-i(\Delta k_x \sin \alpha + \Delta k_y \cos \alpha) d]} \right) \left(\frac{1 - \exp[-i\Delta k_z N_z d]}{1 - \exp[-i\Delta k_z d]} \right). \quad (\text{A17})\end{aligned}$$

It is apparent that $\mathcal{T}_{\text{lattice}}$ will become large if one or more denominators becomes zero. Unfortunately, the three denominators cannot be zero simultaneously. We can choose the first and the third denominators to be zero, i.e., we want:

$$\Delta k_x \cos \alpha - \Delta k_y \sin \alpha = 0, \quad k_z = 0. \quad (\text{A18})$$

We mention that, when $m_a \ll \omega$, we have $\mathbf{k}_a \approx \omega (\cos \theta, \sin \theta \cos \phi, \sin \theta \sin \phi)$. The above relation then becomes:

$$(\omega \cos \theta - k_L) \cos \alpha - \omega \sin \alpha \sin \theta \cos \phi = 0, \quad (a)$$

$$\omega \sin \theta \sin \phi = 0. \quad (b)$$

From Eq.(b) we can have $\phi = 0$. There is still arbitrary in determining the incident angle α , i.e., as long as we have determined the incident angle of the laser α , we can find some specific direction $(\theta(\alpha), \phi = 0)$, on which $\mathcal{T}_{\text{lattice}}$ reaches a maximum. In this paper, we will further add a requirement that $\theta = -\alpha$, i.e., the axion is propagating along x' -direction, so that we have:

$$\cos \alpha = \frac{\omega}{p} = \frac{1}{n}. \quad (\text{A19})$$

Substituting the value of α and $\theta_0 = -\alpha$, $\phi_0 = 0$ into the expression for $\mathcal{T}_{\text{lattice}}$, we have:

$$\mathcal{T}_{\text{lattice}}(\theta_0, \phi_0) = N_x \left(\frac{1 - \exp[iN_x \omega d \tan \alpha]}{1 - \exp[i\omega d \tan \alpha]} \right) N_z \quad (\text{A20})$$

i.e., if we choose the incident angle $\alpha = \arccos \frac{1}{n}$, there will be a coherence peak for axion outgoing in direction (θ_0, ϕ_0) . The height of this peak is proportional to $|\mathcal{T}_{\text{lattice}}|^2 \propto N_x^2 N_z^2$, which means that if the crystal expands on x' and z' direction, the axion number will increase coherently.

3. Two Plane Waves

Now, we are going to rotate the coordinate. In the new coordinate, the cell lattice for the crystal will be aligned along the axis. We will therefore call the new coordinate “crystal coordinate”. The original coordinate will be called “laser coordinate”. In crystal coordinate, the notation will be denoted with a prime, $\mathbf{r}' = (x', y', z')$ and $\mathbf{p}' = (p'_x, p'_y, p'_z)$. The rotation occurs in x - y plane and with angle δ . The forward and backward transformations are:

$$\begin{cases} x' = x \cos \delta + y \sin \delta \\ y' = -x \sin \delta + y \cos \delta \\ z' = z \end{cases}, \quad \begin{cases} x = x' \cos \delta - y' \sin \delta \\ y = x' \sin \delta + y' \cos \delta \\ z = z' \end{cases}. \quad (\text{A21})$$

Similar transformation applies for all vectors. Substituting into Eq.(A10), we have:

$$\tilde{j}'(k_a^0, \mathbf{k}'_a) = -\pi i g_{a\gamma\gamma} B_0 \delta(k_a^0 - \omega) \frac{\Delta k'_x \sin \delta + \Delta k'_y \cos \delta}{\Delta \mathbf{k}'^2} \left[\sum_s q_s e^{-i\Delta \mathbf{k}' \cdot \mathbf{r}'_s} \right]. \quad (\text{A22})$$

If we consider the reflection of laser on the boundary, as shown in the lowermost layer in Fig.1(c), there are two plane wave propagating in the crystal, with wavevectors:

$$\mathbf{k}'_{L1} = n\omega (\cos \alpha, \sin \alpha, 0), \quad \mathbf{k}'_{L2} = n\omega (\cos \alpha, -\sin \alpha, 0). \quad (\text{A23})$$

The corresponding rotation angles are $\delta_1 = \alpha$ and $\delta_2 = -\alpha$, and we have:

$$\tilde{j}'_1(k_a^0, \mathbf{k}'_a) = -\pi i g_{a\gamma\gamma} B_0 \delta(k_a^0 - \omega) \frac{\Delta k'_{1x} \sin \alpha + \Delta k'_{1y} \cos \alpha}{\Delta \mathbf{k}'_1{}^2} \left[\sum_s q_s e^{-i\Delta \mathbf{k}'_1 \cdot \mathbf{r}'_s} \right] \quad (\text{A24})$$

$$\tilde{j}'_2(k_a^0, \mathbf{k}'_a) = -\pi i g_{a\gamma\gamma} B_0 \delta(k_a^0 - \omega) \frac{-\Delta k'_{2x} \sin \alpha + \Delta k'_{2y} \cos \alpha}{\Delta \mathbf{k}'_2{}^2} \left[\sum_s q_s e^{-i\Delta \mathbf{k}'_2 \cdot \mathbf{r}'_s} \right] \quad (\text{A25})$$

where we have defined $\Delta \mathbf{k}'_1 = \mathbf{k}'_a - \mathbf{k}'_{L1}$, $\Delta \mathbf{k}'_2 = \mathbf{k}'_a - \mathbf{k}'_{L2}$.

Substituting into Eq.(A3), the axion number is (we omit the prime notation from now on for short notation, and the following expression is in crystal coordinate):

$$\begin{aligned}
 N_a &= \int \frac{d^3 \mathbf{q}}{(2\pi)^3} \frac{1}{2E_a} \left| \tilde{j}_1(k_a^0, \mathbf{k}_a) + \tilde{j}_2(k_a^0, \mathbf{k}_a) \right|_{k_a^0=E_a}^2 \\
 &= \pi^2 g_{a\gamma\gamma}^2 B_0^2 \frac{T}{2(2\pi)^4} \sqrt{\omega^2 - m_a^2} \int_0^\pi d\theta \int_0^{2\pi} d\phi \\
 &\quad \times \sin \theta \left| \frac{\Delta k_{1x} \sin \alpha + \Delta k_{1y} \cos \alpha}{\Delta \mathbf{k}_1^2} \sum_s q_s e^{-i\Delta \mathbf{k}_1 \cdot \mathbf{r}_s} + \frac{-\Delta k_{2x} \sin \alpha + \Delta k_{2y} \cos \alpha}{\Delta \mathbf{k}_2^2} \sum_s q_s e^{-i\Delta \mathbf{k}_2 \cdot \mathbf{r}_s} \right|^2
 \end{aligned} \tag{A26}$$

The laser comes from the leftmost boundary, and the photon number in corresponding time period is:

$$N_\gamma = \rho_\gamma S v_\gamma T = \frac{B_0^2}{\omega} S \frac{1}{n} T \tag{A27}$$

So we have the transition rate:

$$\begin{aligned}
 P_{\text{laser} \rightarrow a} &= \frac{g_{a\gamma\gamma}^2}{32\pi^2} \frac{n\omega |\mathbf{k}_a|}{S} \int_0^\pi d\theta \int_0^{2\pi} d\phi \\
 &\quad \times \sin \theta \left| \frac{\Delta k_{1x} \sin \alpha + \Delta k_{1y} \cos \alpha}{\Delta \mathbf{k}_1^2} \sum_s q_s e^{-i\Delta \mathbf{k}_1 \cdot \mathbf{r}_s} + \frac{-\Delta k_{2x} \sin \alpha + \Delta k_{2y} \cos \alpha}{\Delta \mathbf{k}_2^2} \sum_s q_s e^{-i\Delta \mathbf{k}_2 \cdot \mathbf{r}_s} \right|^2
 \end{aligned} \tag{A28}$$

Appendix B: Reconversion in Waveguide

We have derived the transition probability from laser to axion. In order to detect those axion, we have to study its conversion back to light signal. With the introducing of axion, the Maxwell equations for the electro-magnetic field are(see, e.g., Ref.[29]):

$$\begin{aligned}
 \nabla \cdot \mathbf{E} &= \frac{\rho}{\varepsilon} - c g_{a\gamma\gamma} \mathbf{B} \cdot \nabla a \\
 \nabla \cdot \mathbf{B} &= 0 \\
 \nabla \times \mathbf{E} &= -\frac{\partial}{\partial t} \mathbf{B} \\
 \nabla \times \mathbf{B} &= \mu \varepsilon \frac{\partial}{\partial t} \mathbf{E} + \mu \mathbf{J} + \frac{g_{a\gamma\gamma}}{c} \left[\frac{\partial a}{\partial t} \mathbf{B} - \mathbf{E} \times \nabla a \right].
 \end{aligned}$$

The electro-magnetic fields inside the crystal can be splitted into two parts: the static, external Coulomb fields inside the crystal, and the propagating fields converted from axion:

$$\mathbf{E} = \mathbf{E}^{\text{ext}} + \mathbf{E}^{\text{prop}}, \quad \mathbf{B} = \mathbf{B}^{\text{prop}},$$

where the \mathbf{E}^{ext} is provided by the ions in ionic crystals. When considering the reconversion process, we neglect the possibility of light transits to axion again. Also, since the regenerated light is very weak and $g_{a\gamma\gamma}$ is very small, we can neglect the $g_{a\gamma\gamma} \mathbf{B}^{\text{prop}}$ and $g_{a\gamma\gamma} \mathbf{E}^{\text{prop}}$ terms. The current \mathbf{J} inside crystal is also ignored. The equations then become (we suppress the upperscript “prop” for shorter notation):

$$\begin{aligned}
 \nabla \times \mathbf{E} &= -\frac{\partial \mathbf{B}}{\partial t} \\
 \nabla \times \mathbf{B} &= \mu \varepsilon \frac{\partial \mathbf{E}}{\partial t} - g_{a\gamma\gamma} \mathbf{E}^{\text{ext}} \times \nabla a \\
 \nabla \cdot \mathbf{E} &= 0 \\
 \nabla \cdot \mathbf{B} &= 0
 \end{aligned}$$

As can be seen, the contribution from axion can be regarded as an effective current \mathbf{J}_{eff} , defined as

$$\mathbf{J}_{\text{eff}}(t, \mathbf{r}) = -\frac{1}{\mu} g_{a\gamma\gamma} \mathbf{E}^{\text{ext}} \times \nabla a. \quad (\text{B1})$$

The regenerated light will be reflected by the boundary of the crystal, which can be regarded as a waveguide. We consider a rectangular waveguide propagating along x -axis, and the cross-section area is $y \in [0, L_y]$, $z \in [0, L_z]$. The phase-match condition from axion production region indicate that the regenerated light will excite the transverse electric (TE) mode of the waveguide, so that the longitudinal electric field, E_x vanishes. The expansion modal of the modes are [30]:

$$E_{ymn}(y, z) = -\frac{2\pi n}{\gamma_{mn} L_z \sqrt{L_y L_z}} \cos\left(\frac{m\pi y}{L_y}\right) \sin\left(\frac{n\pi z}{L_z}\right), \quad (\text{B2})$$

$$E_{zmn}(y, z) = \frac{2\pi m}{\gamma_{mn} L_y \sqrt{L_y L_z}} \sin\left(\frac{m\pi y}{L_y}\right) \cos\left(\frac{n\pi z}{L_z}\right), \quad (\text{B3})$$

$$H_{xmn}(y, z) = -\frac{2i\gamma_{mn}}{k_{mn} Z_{mn} \sqrt{L_y L_z}} \cos\left(\frac{m\pi y}{L_y}\right) \cos\left(\frac{n\pi z}{L_z}\right), \quad (\text{B4})$$

where (m, n) are two indices indicating the different mode, γ_{mn} , k_{mn} and Z_{mn} are given by:

$$\begin{aligned} \gamma_{mn}^2 &= \pi^2 \left(\frac{m^2}{L_y^2} + \frac{n^2}{L_z^2} \right), \\ k_{mn}^2 &= \mu \varepsilon \omega^2 - \gamma_{mn}^2, \\ Z_{mn} &= \mu \omega / k_{mn}. \end{aligned}$$

Since L_y and L_z are large, the integers m and n can be regarded as continuous variable, and so are γ_{mn} and k_{mn} . As we discussed in the main text, the coherence appears for $n = 0$ and $k_{m0} = \omega$. The electric and magnetic component, Eq.(B2-B4) should then be divided by $\sqrt{2}$ to satisfy the normalization condition. Mention that the E_y component disappears for $n = 0$ mode.

The electric field for $(m, 0)$ mode is then:

$$\mathbf{E}(x, y, z, t) = A_{m0} E_{zm0}(y) \hat{\mathbf{z}} e^{-i\omega t + ik_{m0}x} \quad (\text{B5})$$

where the coefficient A_{m0} can be calculated as:

$$A_{m0} = -\frac{Z_{m0}}{2} \int_V d^3\mathbf{r} \mathbf{J}_{\text{eff}}(\mathbf{r}) \cdot \hat{\mathbf{z}} E_{zm0}(y) e^{-ik_{m0}x}, \quad (\text{B6})$$

where V is a large volume containing all the sources \mathbf{J}_{eff} . Notice the minus sign of $e^{-ik_{m0}x}$ in Eq.(B6). The time component of \mathbf{J}_{eff} have been extracted, $\mathbf{J}_{\text{eff}}(t, \mathbf{r}) = \mathbf{J}_{\text{eff}}(\mathbf{r}) e^{-i\omega t}$.

Now we are going to study the source term as in Eq.(B1). The external electric field is provided by the ions inside the ionic crystal. For point particles in free space, the electric field is:

$$\mathbf{E}^{\text{ext}}(\mathbf{r}) = \sum_s \frac{Q_s}{4\pi\varepsilon_0 |\mathbf{r} - \mathbf{r}_s|^3} (\mathbf{r} - \mathbf{r}_s). \quad (\text{B7})$$

Inside medium and waveguide, the electric field should in principle be modified by the medium and also by the boundary condition of the waveguide. However, since the crystal is charge neutral, the electric field far away from any charge will be shielded by another nearby charge with opposite sign. The interaction is significant only in the neighbourhood of the charges, where the boundary condition and medium effect is not important. We will therefore use the free-space form of the charges.

For the axion field, we consider it to be a plane wave propagating along x -axis:

$$a(t, \mathbf{r}) = a_0 e^{-i\omega t + i\mathbf{p}_a \cdot \mathbf{r}} \quad (\text{B8})$$

where $\mathbf{p}_a = (p_a, 0, 0)$. Substituting into Eq.(B1), we have the source term:

$$\mathbf{J}_{\text{eff}}(\mathbf{r}) = -\frac{i}{\mu} g_{a\gamma\gamma} a_0 e^{i\mathbf{p}_a \cdot \mathbf{r}} \mathbf{E}^{\text{ext}}(\mathbf{r}) \times \mathbf{p}_a. \quad (\text{B9})$$

Then, using Eq.(B6), we can derive the amplitude:

$$A_{m0} = \frac{\sqrt{2}}{2} \frac{ig_{a\gamma\gamma} a_0}{\sqrt{L_y L_z}} \frac{\omega}{k_{m0} \varepsilon_0} p_a \sum_s Q_s e^{i(p_a - \omega)x_s + iq_y y_s} \frac{q_y}{(p_a - \omega)^2 + q_y^2} \quad (\text{B10})$$

where $q_y = m\pi/L_y$. By carefully choosing the mode, we can have $k_{m0} = \omega$, and $q_y = \sqrt{n^2 - 1}\omega$, to satisfy the coherence.

The transverse magnetic field is:

$$\mathbf{H}_t = \frac{1}{Z} \hat{\mathbf{x}} \times \mathbf{E}_t. \quad (\text{B11})$$

For $(m, 0)$ mode, the electric field only has z -component, so the transverse magnetic field only has y -component (together with longitudinal H_x component). The Poynting vector of the regenerated light is then (an extra 1/2 factor for averaging over time):

$$\langle \mathbf{S} \rangle = \frac{1}{2} \mathbf{E} \times \mathbf{H}^* = \frac{1}{2Z_{m0}} E_z^2 \hat{\mathbf{x}}. \quad (\text{B12})$$

For a cross sectional area $S = L_y L_z$, we integrate over S and obtain the averaged power:

$$\langle P_{\text{waveguide}} \rangle = \int dy dz \langle S_x \rangle \quad (\text{B13})$$

For a plane wave of axion, the time-averaged energy density is:

$$\langle \rho_a \rangle = \frac{1}{2} a_0^2 (\mathbf{p}_a^2 + m_a^2) = \frac{1}{2} a_0^2 \omega^2, \quad (\text{B14})$$

and the power for axion across cross sectional area S is:

$$\langle P_a \rangle = \frac{1}{2} a_0^2 \omega^2 v_a S \quad (\text{B15})$$

So the conversion probability is:

$$P_{a \rightarrow \gamma} \equiv \frac{\langle P_{\text{waveguide}} \rangle}{\langle P_a \rangle} = \frac{1}{2\mu} \frac{g_{a\gamma\gamma}^2}{\varepsilon_0^2 \omega^2 v_a S^2} \frac{p_a^2 q_y^2}{\mathbf{k}^4} \left| \sum_s Q_s e^{i(p_a - \omega)x_s + iq_y y_s} \right|^2 \quad (\text{B16})$$

where for maximum coherence, we have already require:

$$\begin{aligned} k_{m0} &= \omega, \\ Z_{m0} &= \mu. \end{aligned}$$

Appendix C: Contribution from In-Atom Electric Field

Throughout this paper, we have been treating the ions as point charges. However, the ions have finite size and the electric field inside those ions can be much larger than the inverse-square Coulomb field, since the nucleons have

larger charge. One may expect that these larger electric field might contribute to extra axion production. However, in this section, we will show that those contribution is negligible for long-wavelength optical light.

For an ion whose nuclear charge is Z_s , total charge number is Q_s (i.e., with $Z_s - Q_s$ electrons) and radius is R_s , we model it as a pure nucleus surrounded by electron cloud. The electric field from the nucleus is:

$$\mathbf{E}_s^{\text{nucl}} = \frac{Z_s e}{4\pi |\mathbf{r} - \mathbf{r}_s|^3} (\mathbf{r} - \mathbf{r}_s).$$

The electron cloud is considered to be uniformly distributed inside a sphere with radius R_s . Inside the sphere, the electric field can be derived using Gauss law, while the electric field outside the sphere is the same as point charge:

$$\begin{aligned} \mathbf{E}_s^e &= -\frac{(Z_s - Q_s)e}{4\pi R_s^3} (\mathbf{r} - \mathbf{r}_s) \Theta(R_s - |\mathbf{r} - \mathbf{r}_s|) - \frac{(Z_s - Q_s)e}{4\pi |\mathbf{r} - \mathbf{r}_s|^3} (\mathbf{r} - \mathbf{r}_s) \Theta(|\mathbf{r} - \mathbf{r}_s| - R_s) \\ &= -\frac{(Z_s - Q_s)e}{4\pi} (\mathbf{r} - \mathbf{r}_s) \Theta(R_s - |\mathbf{r} - \mathbf{r}_s|) \left[\frac{1}{R_s^3} - \frac{1}{|\mathbf{r} - \mathbf{r}_s|^3} \right] - \frac{(Z_s - Q_s)e}{4\pi |\mathbf{r} - \mathbf{r}_s|^3} (\mathbf{r} - \mathbf{r}_s), \end{aligned}$$

where Θ is the step function.

The total electric field is then the sum of contribution from nucleus and electron:

$$\begin{aligned} \mathbf{E}_s &= \mathbf{E}_s^{\text{nucl}} + \mathbf{E}_s^e \\ &= \frac{Q_s e}{4\pi |\mathbf{r} - \mathbf{r}_s|^3} (\mathbf{r} - \mathbf{r}_s) - \frac{(Z_s - Q_s)e}{4\pi} (\mathbf{r} - \mathbf{r}_s) \Theta(R_s - |\mathbf{r} - \mathbf{r}_s|) \left[\frac{1}{R_s^3} - \frac{1}{|\mathbf{r} - \mathbf{r}_s|^3} \right] \\ &\equiv \mathbf{E}_s^{\text{point}} + \mathbf{E}_s^{\text{in-ion}}, \end{aligned}$$

where we have defined:

$$\begin{aligned} \mathbf{E}_s^{\text{point}} &= \frac{Q_s e}{4\pi |\mathbf{r} - \mathbf{r}_s|^3} (\mathbf{r} - \mathbf{r}_s), \\ \mathbf{E}_s^{\text{in-ion}} &= -\frac{(Z_s - Q_s)e}{4\pi} (\mathbf{r} - \mathbf{r}_s) \Theta(R_s - |\mathbf{r} - \mathbf{r}_s|) \left[\frac{1}{R_s^3} - \frac{1}{|\mathbf{r} - \mathbf{r}_s|^3} \right]. \end{aligned}$$

It is clear that $\mathbf{E}_s^{\text{point}}$ is the point charge contribution as we have used in the main text and in Appendix A, and $\mathbf{E}_s^{\text{in-ion}}$ is the modification from the electric field inside ions.

For simplicity, we consider a circularly polarized laser propagating along x -direction inside the medium. The corresponding \mathbf{B} component is:

$$\mathbf{B} = (0, B_0 \cos(\omega t - k_L x), B_0 \sin(\omega t - k_L x)),$$

where $k_L = n\omega$ with refractive index $n > 1$.

The classical source for axion in Eq. (1) is then

$$\begin{aligned} j(t, \mathbf{r}) &= \sum_s g_{a\gamma\gamma} \mathbf{E}_s^{\text{point}} \cdot \mathbf{B} + \sum_s g_{a\gamma\gamma} \mathbf{E}_s^{\text{in-ion}} \cdot \mathbf{B} \\ &\equiv j^{\text{point}}(t, \mathbf{r}) + j^{\text{in-ion}}(t, \mathbf{r}), \end{aligned}$$

where the $j^{\text{point}}(t, \mathbf{r})$ term can be derived following Appendix A, except that we use circularly polarized laser here. The Fourier transformation of j^{point} should then be:

$$\tilde{j}^{\text{point}}(k_a^0, \mathbf{k}_a) = -\frac{\pi}{2} g_{a\gamma\gamma} B_0 e^{i\phi} \delta(k_a^0 - \omega) \sum_s Q_s e^{-i(\mathbf{k}_a - \mathbf{k}_L) \cdot \mathbf{r}_s} \frac{2|\mathbf{k}_a| \sin \theta}{(\mathbf{k}_a - \mathbf{k}_L)^2}, \quad (\text{C1})$$

where θ is the polar angle between \mathbf{k}_a and x -axis (mention that \mathbf{k}_L is along x -axis), and ϕ is the azimuthal angle. The angles are defined through $k_{ax} = |\mathbf{k}_a| \cos \theta$, $k_{ay} = |\mathbf{k}_a| \sin \theta \cos \phi$, $k_{az} = |\mathbf{k}_a| \sin \theta \sin \phi$.

In order to calculate the axion conversion probability, we need then derive $j^{\text{in-ion}}$ term. The Fourier transformation of the source is:

$$\begin{aligned}\tilde{j}^{\text{in-ion}}(k_a^0, \mathbf{k}_a) &= - \int dt d^3\mathbf{r} \exp[itk_a^0 - i\mathbf{k}_a \cdot \mathbf{r}] j^{\text{in-ion}}(t, \mathbf{r}) \\ &= - \frac{g_a \gamma \gamma B_0 e}{4} \delta(k_a^0 - \omega) \sum_s (Z_s - Q_s) e^{-i\mathbf{k}_a \cdot \mathbf{r}_s} e^{ik_L x_s} \\ &\quad \times \left\{ \int d^3\mathbf{r} e^{-i\mathbf{k}_a \cdot \mathbf{r}} e^{ik_L x} (y + iz) \left(\frac{1}{R_s^3} - \frac{1}{|\mathbf{r}|^3} \right) \Theta(R_s - |\mathbf{r}|) \right\}\end{aligned}$$

The terms in the curly bracket is the contribution for a single ion at origin. The integration over $d^3\mathbf{r}$ is the corresponding Fourier transformation. For short notation, we define:

$$\begin{aligned}j_s^{\text{in-ion}}(\mathbf{r}) &= e^{ik_L x} (y + iz) \left(\frac{1}{R_s^3} - \frac{1}{|\mathbf{r}|^3} \right) \Theta(R_s - |\mathbf{r}|), \\ \tilde{j}_s^{\text{in-ion}}(\mathbf{k}_a) &= \int d^3\mathbf{r} \exp[-i\mathbf{k}_a \cdot \mathbf{r}] j_s^{\text{in-ion}}(\mathbf{r}),\end{aligned}\tag{C2}$$

and we have:

$$\Rightarrow \tilde{j}^{\text{in-ion}}(k_a^0, \mathbf{k}_a) \equiv - \frac{g_a \gamma \gamma B_0 e}{4} \delta(k_a^0 - \omega) \sum_s (Z_s - Q_s) e^{-i\mathbf{k}_a \cdot \mathbf{r}_s} e^{ik_L x_s} \tilde{j}_s^{\text{in-ion}}(\mathbf{k}_a)\tag{C3}$$

We are going to use cylindrical coordinate, $\mathbf{r} = (x, y, z) = (x, \rho, \psi)$, where $\rho = \sqrt{y^2 + z^2}$, $y = \rho \cos \psi$ and $z = \rho \sin \psi$. The Fourier transformation can also be written in cylindrical coordinate, i.e., $\mathbf{k}_a = (k_{ax}, k_{ay}, k_{az}) = (k_{ax}, k_{a\rho}, \phi)$, where $k_{a\rho} = \sqrt{k_{ay}^2 + k_{az}^2}$, $k_{ay} = k_{a\rho} \cos \phi$ and $k_{az} = k_{a\rho} \sin \phi$. As shown in Ref.[28], the Fourier transformation in cylindrical coordinate should be written as:

$$\tilde{j}_s^{\text{in-ion}}(k_{ax}, k_{a\rho}, \phi) = - 2\pi i e^{i\phi} \int dx e^{-i(k_{ax} - k_L)x} \int_0^\infty \rho^2 d\rho \left(\frac{1}{R_s^3} - \frac{1}{(x^2 + \rho^2)^{3/2}} \right) \Theta(R_s - (x^2 + \rho^2)^{1/2}) J_1(k_{a\rho}\rho),\tag{C4}$$

where J_1 is the first order Bessel function.

This integration cannot be integrated analytically. However, if we use optical light, the wavelength λ is far larger than the atom radius R_s . We therefore have $|\mathbf{k}_a| R_s, k_{ax} R_s, k_{a\rho} R_s \ll 1$ and the Bessel function approaches its asymptotic expression:

$$J_\alpha(z) \sim \frac{1}{\Gamma(\alpha + 1)} \left(\frac{z}{2} \right)^\alpha, \quad 0 < z \ll \sqrt{\alpha + 1}.$$

We can then perform the integration in Eq.(C4) and approximately have:

$$\tilde{j}_s^{\text{in-ion}}(k_{ax}, k_{a\rho}, \phi) \approx - 4\pi i e^{i\phi} \frac{k_\rho}{(k_{ax} - k_L)^5 R_s^3} \left[(k_{ax} - k_L)^3 R_s^3 + 3(k_{ax} - k_L) R_s \cos((k_{ax} - k_L) R_s) - 3 \sin((k_{ax} - k_L) R_s) \right]$$

As we have stated, $(k_{ax} - k_L) R_s \ll 1$. We can then further approximate the sin and cos function in this limit and have:

$$\tilde{j}_s^{\text{in-ion}}(k_{ax}, k_{a\rho}, \phi) \approx - 4\pi i e^{i\phi} k_\rho R_s^2\tag{C5}$$

Substituting Eq.(C5) into Eq.(C3), the complete Fourier transformation for in-ion contribution is:

$$\tilde{j}^{\text{in-ion}}(k_a^0, \mathbf{k}_a) = \pi i g_{a\gamma\gamma} B_0 e^{i\phi} \delta(k_a^0 - \omega) \sum_s (Z_s - Q_s) e^{-i(\mathbf{k}_a - \mathbf{k}_L) \cdot \mathbf{r}_s} |\mathbf{k}_a| \sin \theta R_s^2$$

The point-charge contribution is given in Eq.(C1), and the total source term is

$$\begin{aligned} \tilde{j}(k_a^0, \mathbf{k}_a) &= \tilde{j}^{\text{point}}(k_a^0, \mathbf{k}_a) + \tilde{j}^{\text{in-ion}}(k_a^0, \mathbf{k}_a) \\ &= -\pi g_{a\gamma\gamma} B_0 e^{i\phi} \delta(k_a^0 - \omega) \frac{|\mathbf{k}_a| \sin \theta}{(\Delta \mathbf{k})^2} \sum_s e^{-i\Delta \mathbf{k} \cdot \mathbf{r}_s} \left\{ Q_s - (Z_s - Q_s) (\Delta \mathbf{k})^2 R_s^2 \right\}, \end{aligned} \quad (\text{C6})$$

where $\Delta \mathbf{k} = \mathbf{k}_a - \mathbf{k}_L$ is the momentum transfer. The first term in the curly bracket is the result from point-charge approximation, and the second term in the curly bracket comes from the modification of in-ion electric field. Mention that the wavelength of the laser is of order $\lambda \approx 2\pi/|\Delta \mathbf{k}| \sim 10^{-6}\text{m}$, while the radius of atom is of order $R_s \sim 10^{-10} - 10^{-9}\text{m}$. The modification from the in-ion electric field is of order $(R_s/\lambda)^2$.

However, considering that the crystal is charge neutral, there is a cancellation in the point-charge term. As in Eq.(3) in the main text, the point-charge term can be split into two component:

$$\sum_s e^{-i\Delta \mathbf{k} \cdot \mathbf{r}_s} Q_s = \left\{ \sum_c e^{-i\Delta \mathbf{k} \cdot \delta \mathbf{r}_c} Q_c \right\} \left\{ \sum_l e^{-i\Delta \mathbf{k} \cdot \mathbf{r}_l} \right\},$$

where the first term is the contribution from a single cell and the subscript c runs over all charges inside one cell, the second term is the contribution from entire lattice and the subscript l runs over all the lattice cells. $\delta \mathbf{r}_c$ is the relative coordinate of charges inside one cell. Apparently, since the crystal is charge neutral, we have $\sum_c Q_c = 0$. However, the spatial translation of charges provide extra phases, and we have:

$$\sum_c e^{-i\Delta \mathbf{k} \cdot \delta \mathbf{r}_c} Q_c \approx i |\Delta \mathbf{k}| d,$$

where d is the crystal lattice constant and we have used the expansion $\exp(-i\Delta \mathbf{k} \cdot \delta \mathbf{r}_c) \approx 1 - (i\Delta \mathbf{k} \cdot \delta \mathbf{r}_c)$. Considering that we have $|\Delta \mathbf{k}| \approx 2\pi/\lambda$, the first term in the curly bracket of (C6) damps as d/λ . The ion radius R_s is comparable to lattice constant d , so the second term in the curly bracket of (C6) is smaller than the first term by a factor of $d/\lambda \approx 10^{-3}$, so we can safely omit the second term, i.e. the contribution from in-ion electric field can be ignored.

We also mention that, if we take $Q_s = 0$, the result corresponds to axion production from charge-neutral atoms. Therefore, the contribution from the supporting material in Fig.1(c) is negligible due to the R_s/λ suppression.